

Effects of Spray Configuration on the Uniformity of Cooling Rate and Hardness in the Quenching of Aluminum Parts with Nonuniform Shapes

J.C. Rozzi, W.P. Klinzing, and I. Mudawar

The present study constitutes a step toward the understanding, and eventual optimization, of the spray quenching process for aluminum extrusions. A spray quenching test bed was constructed to simulate an industrial spray quench. This experimental facility allowed for the testing of irregular shapes using up to eight water sprays. Quenching experiments were conducted using flat water sprays in two different configurations with an L-shape testpiece constructed from commercially pure aluminum Al 1100-O. Section thickness and spray configuration were found to have a significant effect on the cooling rate and cooling uniformity. The commercially pure aluminum Al 1100-O L-shape and a similar L-shape constructed from aluminum alloy 2024-T6 were simulated with a two-dimensional finite-element code and spray correlations available from previous studies. Using the quench factor technique, the numerical simulation enabled the assessment of merits of different spray configurations with respect to the magnitude and uniformity of hardness of the 2024-T6 L-shape.

1 Introduction

MATERIALS processing is increasingly becoming one of the most formidable challenges facing many industries. With rapid advances in technology, more reliable and more fully characterizable materials are needed to meet increasingly tougher specifications. Spray quenching of aluminum alloys is a prime example of a process and material that require improvement because of the high performance requirements demanded by, for example, the aerospace industry.

Typically, an aluminum extrusion is cooled by a deluge of water sprays on exiting the extrusion die. This renders extrusion, more or less, a continuous process that does not involve many line changes. Extrusion is therefore a cost-effective method of manufacturing aluminum alloys, limited only by the size of the original aluminum billet that can be placed in the extrusion press.

At present, the method of placing the water sprays relative to the extrusion is one of trial and error, guided by the visual appearance of the extrusion and the operator experience and intuition. Soft spots, surface degradation, and warpage are a few examples of the many undesirable outcomes of improper placement of the sprays. Furthermore, if warpage occurs, the material must be straightened back to the desired shape. This post-extrusion process is not only costly, but it induces residual stresses within the material. The effects of this post-extrusion step on the final product can seldom be accounted for with certainty. The logical answer to this problem is the development of an intelligent spray quenching technology, making use of the recent revolutionary advances in computer-aided design (CAD). Given the cross section and desired material properties of the extrusion, a CAD system could be developed that would determine the

proper spray nozzle location and pressure to achieve optimum cooling. The present research constitutes a step toward achieving this goal.

Material properties are influenced both by the quenching and subsequent aging of the alloy. The effect of quench rate on the age hardenability of an aluminum alloy is illustrated in Fig. 1(a). A rapid quench preserves the original microstructure, producing an alloy that is age hardenable and, potentially, possessing maximum strength and hardness. However, even if the quench is sufficiently fast, there remains the danger of overaging the material. With overaging, precipitates begin to coalesce, resulting in a reduced number of barriers to dislocations. The strength and hardness of the material therefore decreases. Proper aging and overaging, along with the resulting microstructure, are shown in Fig. 1(b).

Given these age hardenability considerations alone, a fast quench at every point within the extrusion seems quite desirable. However, from a practical standpoint, this is impossible. Because the quenching process is a surface phenomenon, points on or near the quenched surface may be cooled rapidly enough to achieve the maximum strength and hardness, whereas deep within the part a slower quench will take place, resulting in poorer mechanical properties on age hardening. Furthermore, the large thermal gradients produced during a fast quench can cause warping and large residual stresses, especially with parts having irregular shapes and large variations in thickness, *i.e.*, large variations in thermal mass. Therefore, a tradeoff exists between maximizing strength and hardness on one hand and minimizing warping and residual stresses, hence the notion of the window of acceptable cooling rate.^[2] However, before this tradeoff can be made, knowledge of how the quenching process affects the final material properties becomes vital.

One measure of the quality of an alloy quench as it relates to the material hardness and yield strength is known as the quench factor, τ . The quench factor enables the calculation of hardness and yield strength at points within the quenched part, provided both the time-temperature-transformation curve (the *C*-curve)

J.C. Rozzi, Graduate Research Assistant, W.P. Klinzing, Graduate Research Assistant, and I. Mudawar, Associate Professor and Director, Boiling and Two-Phase Flow Laboratory, School of Mechanical Engineering, Purdue University, West Lafayette, Indiana.

Nomenclature

- C_t = critical time, sec
 c_p = specific heat, J/kg · K
 d_{32} = Sauter mean diameter (SMD), m
 H = hardness
 h = convection coefficient, W/m² · K
 h_{fg} = latent heat of vaporization, J/kg
 k = thermal conductivity, W/m · K
 k_1 = constant equal to the natural logarithm of the untransformed portion of precipitate
 Nu_{32} = Nusselt number based on Sauter mean diameter, $h d_{32}/k_f$
 Pr = Prandtl number
 q'' = heat flux, W/m²
 q''_{CHF} = critical heat flux, W/m²
 Q'' = volumetric flux, m³ sec⁻¹/m²
 Re_{32} = Reynolds number based on volumetric flux and Sauter mean diameter, $Q'' d_{32}/\nu_f$
 t = time, sec
 T = temperature, °C
 T_{CHF} = temperature corresponding to critical heat flux, °C
 T_{DFB} = temperature corresponding to departure from film boiling, °C
 T_{MIN} = temperature corresponding to minimum heat flux, °C
 U_m = mean drop velocity, m/sec
 X = spatial coordinate
 Y = spatial coordinate

Greek Symbols

- $\Delta T = T_s - T_f$, °C
 $\Delta T_{sat} = T_s - T_{sat}$, °C
 $\Delta T_{sub} = T_{sat} - T_f$, °C
 ν = kinematic viscosity, m²/sec
 ρ = density, kg/m³
 σ = surface tension, N/m
 σ' = yield strength, MPa
 τ = quench factor

Subscripts

- CHF = critical heat flux
 DFB = departure from film boiling
 f = liquid
 g = vapor
 max = maximum
 min = minimum
 MIN = minimum heat flux
 s = surface
 sat = saturation
 sub = subcooled

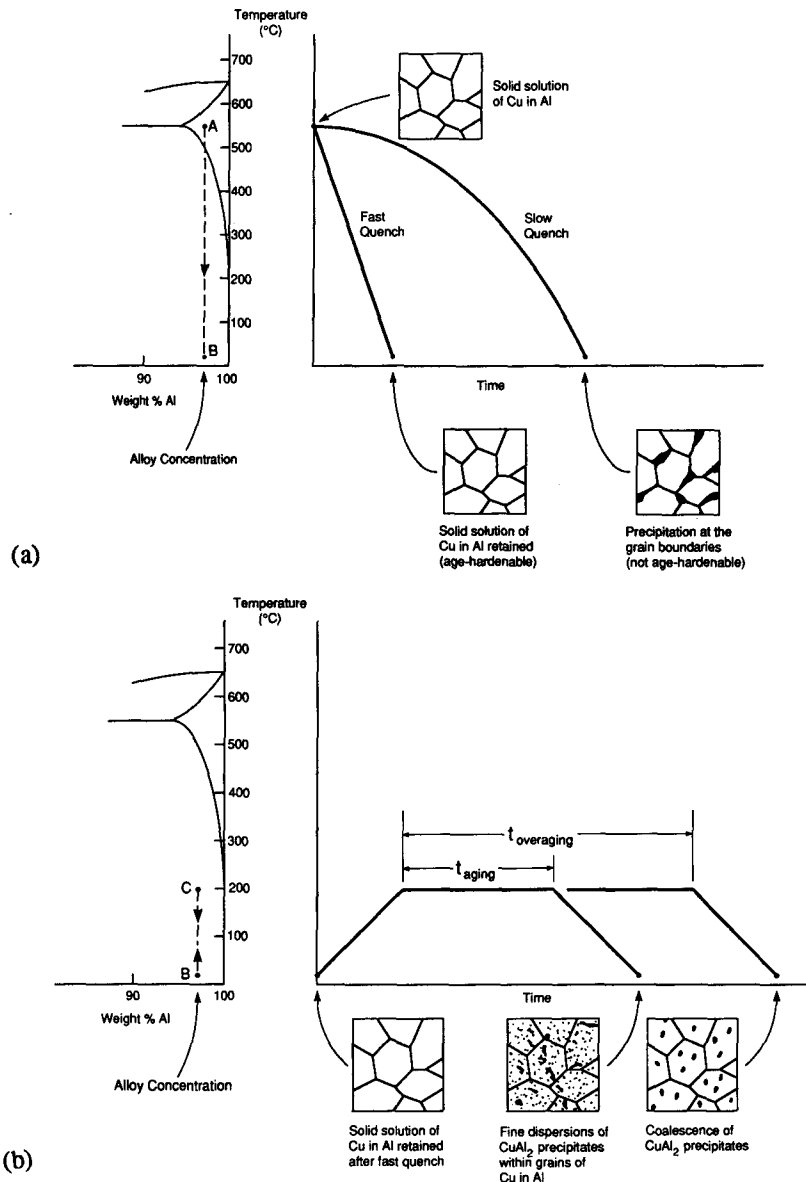


Fig. 1 Effects of the (a) quenching and (b) aging processes on the final material microstructure. Adapted from Shackelford.^[1]

and the temperature-time-cooling curve (the boiling curve) are known.

For a quench factor analysis to be valid in the transient nonisothermal quenching of an alloy, the reaction that takes place from the solvus temperature to room temperature must be additive.^[3] As indicated by Cahn,^[4] a reaction is additive when the reaction rate is a function of only the amount of transformation, x , from, in the case of an aluminum-copper alloy, the solid solution of copper in aluminum to the new phase of CuAl_2 within the solid solution of copper in aluminum, and the temperature, T :

$$\frac{dx}{dt} = f(x, T) \quad [1]$$

This is true for certain metals and alloys such as aluminum alloy 2024-T6.^[5] For additive reactions, Cahn^[4] defined the quench factor for a continuous cooling process between times t_0 and t_f as a measure of the amount of material transformed during the same period:

$$\int_{t_0}^{t_f} \frac{dt}{C_t} = \tau \quad [2]$$

Evancho and Staley^[3] developed a technique for relating the quench factor, de-

finned in Eq 2, to isothermal precipitation kinetics for aluminum alloys as well as final material properties. They defined the yield strength ratio as:

$$YSR = \frac{\sigma' - \sigma'_{\min}}{\sigma'_{\max} - \sigma'_{\min}} = \exp(k_1 \tau) \quad [3]$$

where k_1 is a negative constant equal to the natural logarithm of the untransformed portion of precipitate. An analogous relationship was defined for the hardness ratio by Kim:^[5]

$$HR = \frac{H - H_{\min}}{H_{\max} - H_{\min}} = \exp(k_1 \tau) \quad [4]$$

Because k_1 is negative, high values of the yield strength and hardness correspond to small values of τ . Given the C -curve for the alloy in question and the temperature-time-cooling curve, the quench factor, and therefore, the yield strength and hardness can be calculated using Eq 2, 3, and 4, respectively. Because the temperature-time-cooling curve depends on both the thermal mass of the alloy and the spray conditions, the quench factor enables interrelation of the effects of part shape, section thickness, and spray conditions, and assessment of their effect on the yield strength and hardness.^[6] However, to calculate the quench factor, one must first be able to determine the temperature-time-cooling curve at points of interest within the quenched part. Using this information, the integral in Eq 2 can be computed, giving the quench factor value at the point corresponding to the temperature-time-cooling curve.

When a metal or alloy is quenched, whether it be in a stagnant bath of liquid or by a liquid spray, depending on its initial temperature, it experiences all or most of the regimes associated with the boiling curve. Such a curve is shown in Fig. 2, which is for the case of a hot surface in a stagnant pool of liquid at its saturation temperature. The figure shows the wall heat flux, q'' , plotted against the surface temperature excess above liquid saturation, ΔT_{sat} . Upon traversing the boiling curve from high temperature to low, the transition between boiling regimes is accompanied by large changes in the heat flux and corresponding large changes in cooling rate. Therefore, the characterization of these regimes is of paramount importance to material processing. The point of minimum heat flux is of particular significance to the final material properties, because it marks the onset of rapid cooling.

A series of studies conducted at the Purdue University Boiling and Two-Phase Flow Laboratory^[7-9] has culminated in heat transfer correlations characterizing the boiling curve for spray quenching with respect to the spray volumetric flux, Q'' , Sauter mean drop diameter, d_{32} , and mean drop velocity, U_m , all measured locally in the spray field. Volumetric flux, Q'' , is defined as the local volume flow rate of water per unit surface area. The Sauter mean diameter and mean drop velocity are statistical measures of the drop volume-to-surface area ratio and the drop momentum per unit mass, respectively. Given a large sample of drops, these two parameters are defined, respectively, as:

$$d_{32} \equiv \frac{\sum n_i d_i^3}{\sum n_i d_i^2} \quad [5]$$

$$U_m \equiv \frac{\sum n'_i \rho_f u_{d,i} \left(\frac{d_i^3}{6} \right)}{\sum n'_i \rho_f \left(\frac{d_i^3}{6} \right)} \quad [6]$$

where n_i is the number of drops of diameter d_i , and n'_i is the number of drops of diameter d_i traveling at velocity $u_{d,i}$ perpendicular to the quenched surface. The correlations developed in the above cited heat transfer studies are given in Table 1.

The present study constitutes a step toward developing a methodology for optimizing the quenching of aluminum alloy parts with nonuniform shapes. The effects of spray configuration on the quenching of an L-shape part are investigated both experimentally and computationally. Hardness distributions are presented to illustrate the sensitivity of material properties to the spray configuration for a simulated quench of an Al 2024-T6 L-shape part.

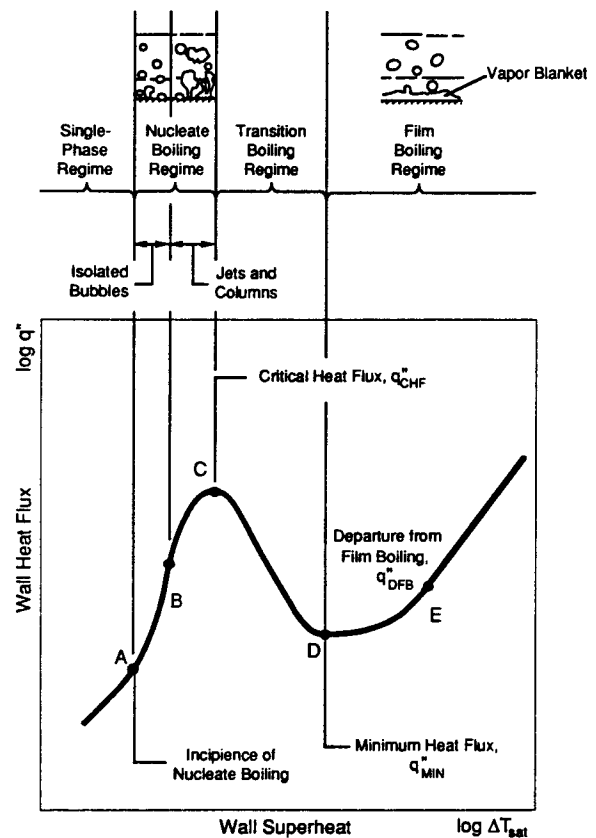


Fig. 2 Boiling curve for a hot surface in a stagnant pool of liquid at its saturation temperature.

Table 1 Summary of Spray Heat Transfer Correlations

Boiling (quenching) regime	Correlation
Film boiling ^[8]	$Q'' > 3.5 \times 10^{-3}$: $q'' = 1.413 \times 10^5 \Delta T^{0.461} Q''^{0.566} U_m^{0.639}$ $Q'' < 3.5 \times 10^{-3}$: $q'' = 63.250 \Delta T^{1.691} Q''^{0.264} d_{32}^{-0.062}$
Point of departure from film boiling ^[9]	$Q'' > 3.5 \times 10^{-3}$: $q''_{DFB} = 6.536 \times 10^6 Q''^{0.995} U_m^{0.924}$ $\Delta T_{DFB} = 3.079 \times 10^4 Q''^{-0.194} U_m^{1.922} d_{32}^{1.651}$ $Q'' < 3.5 \times 10^{-3}$: $q''_{DFB} = 6.100 \times 10^6 Q''^{0.588} U_m^{0.244}$ $\Delta T_{DFB} = 2.808 \times 10^2 Q''^{0.087} U_m^{0.110} d_{32}^{-0.035}$
Film-wetting regime ^[9]	$q'' = N_0 + N_1 \Delta T + N_2 \Delta T^2$ $N_0 = q''_{MIN} - N_1 \Delta T_{MIN} - N_2 \Delta T_{MIN}^2$ $N_1 = -2N_2 \Delta T_{MIN}$ $N_2 = \frac{q''_{DFB} - q''_{MIN}}{(\Delta T_{DFB} - \Delta T_{MIN})^2}$
Minimum heat flux ^[9]	$Q'' > 3.5 \times 10^{-3}$: $q''_{MIN} = 6.069 \times 10^6 Q''^{0.943} U_m^{0.864}$ $\Delta T_{MIN} = 7.990 \times 10^3 Q''^{-0.027} U_m^{1.330} d_{32}^{0.952}$ $Q'' < 3.5 \times 10^{-3}$: $q''_{MIN} = 3.324 \times 10^6 Q''^{0.544} U_m^{0.324}$ $\Delta T_{MIN} = 2.049 \times 10^2 Q''^{0.066} U_m^{0.138} d_{32}^{-0.035}$
Transition boiling ^[9]	$q'' = q''_{CHF} - \frac{q''_{CHF} - q''_{MIN}}{(\Delta T_{CHF} - \Delta T_{MIN})^3} \left[\Delta T_{CHF}^3 - 3\Delta T_{CHF}^2 \Delta T_{MIN} + 6\Delta T_{CHF} \Delta T_{MIN} \Delta T - 3(\Delta T_{CHF} + \Delta T_{MIN}) \Delta T^2 + 2\Delta T^3 \right]$
Critical heat flux ^[7]	$\frac{q''_{CHF}}{\rho_g h_{fg} Q''} = 122.4 \left[1 + 0.0118 \left(\frac{\rho_f}{\rho_g} \right)^{1/4} \left(\frac{\rho_f c_{p,f} \Delta T_{sub}}{\rho_g h_{fg}} \right) \right] \left(\frac{\sigma}{\rho_f Q''^2 d_{32}} \right)^{0.198}$ $\Delta T_{CHF} = 18 \left[(\rho_g h_{fg} Q'') \left(\frac{\sigma}{\rho_f Q''^2 d_{32}} \right)^{0.198} \right]^{1/3.55}$
Nucleate boiling ^[7]	$q'' = 1.87 \times 10^{-5} (\Delta T)^{5.55}$
Incipient boiling ^[7]	$\Delta T = 13.43 Re_{32}^{0.167} Pr_f^{0.123} \left(\frac{k_f}{d_{32}} \right)^{0.220}$
Single-phase cooling ^[7]	$Nu_{32} = 2.512 Re_{32}^{0.167} Pr_f^{0.56}$

Note: Units of the parameters are q'' (W/m²), ΔT (°C), Q'' (m³sec⁻¹/m²), U_m (m/sec), d_{32} (m), ρ_f (kg/m³), ρ_g (kg/m³), $c_{p,f}$ (J/kg · K), h_{fg} (J/kg), σ (N/m). Ranges of validity of the correlations are $Q'' = 0.6$ to 9.96×10^{-3} m³ sec⁻¹/m², $U_m = 10.1$ to 26.7 m/sec and $d_{32} = 405 \times 10^{-3}$ to 1350×10^{-3} m, $T_f = 23$ °C.

2 Experimental Methods

2.1 Quenching Test Bed

The quenching test bed constructed for this study was designed to accommodate the hardware necessary for simulating an industrial spray quench. Major components of the test bed included a support structure, furnace, testpiece translation apparatus, spray chamber, exhaust system, and fluid delivery loop, all of which are shown schematically in Fig. 3. Because of the large size of the test bed, many of the components required structural support. For this reason, the upper platform, upon which the furnace was supported, as well as the tall legs that extended downward, were constructed of heavy-duty cold rolled carbon steel square tubing. The stand for the large reservoir was constructed of the same tubing along with carbon steel angle. The legs of both the furnace and reservoir support structures were first

bolted together and then bolted onto a welded steel weight distribution pad. This ensured total system fit and stability.

The testpiece was heated in a three-zone tube furnace with a 60.96-cm (24-in.) heated length. The three zones of heating and long heated length facilitated uniform heat-up of the testpiece. The furnace was bolted to the upper platform with its lower end approximately 3.05 m (10 ft) from floor level. A process tube was mounted inside the furnace to protect the furnace heating elements during testing, as shown in Fig. 4(a). The lower opening of the furnace was sealed with an insulating plug that was carried on the platform used to transport the testpiece to the furnace. The upper opening of the furnace was sealed with a stationary plug made of the same insulating material as the lower plug.

The testpiece platform was constructed of carbon steel plate and is illustrated in Fig. 4(b). On the platform were placed four short stainless steel spacers that supported a stainless steel plate. The spacers served to reduce heat transfer between the stainless

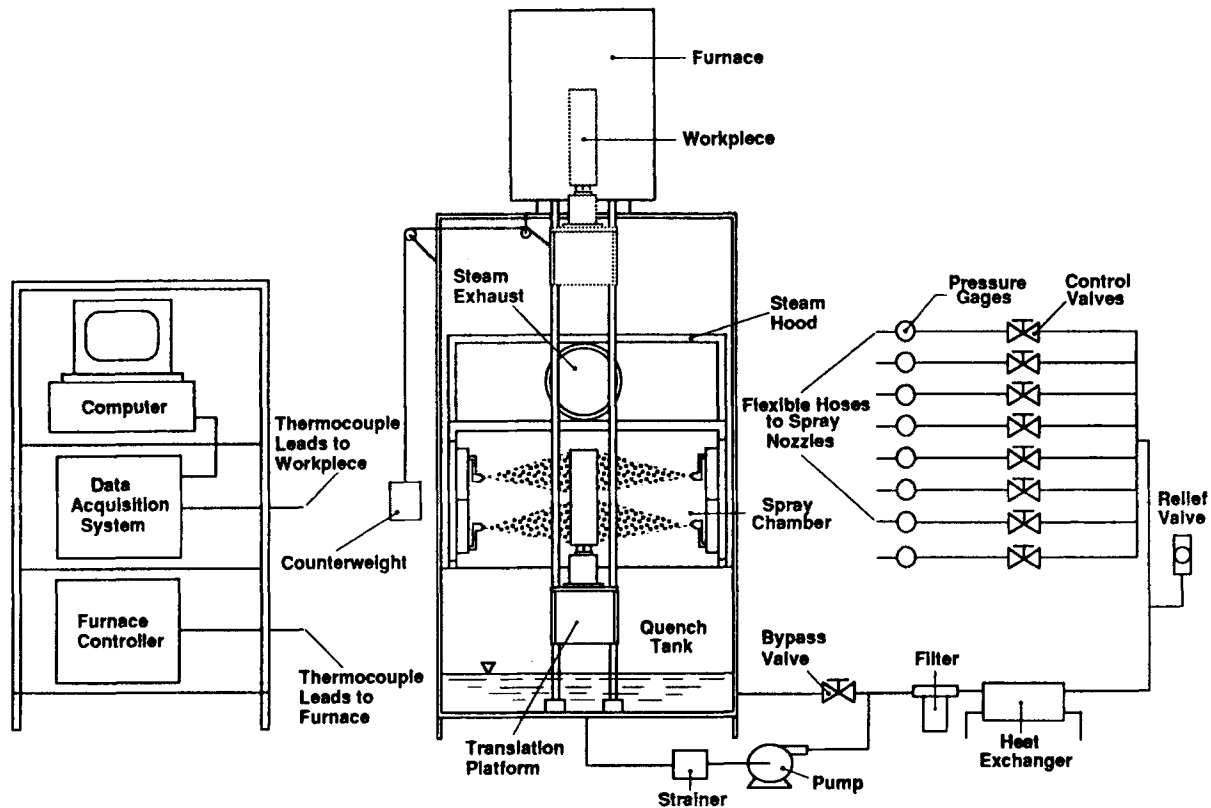


Fig. 3 Schematic of quenching test bed.

steel plate and the lower parts of the platform by minimizing contact area. The stainless steel plate was countersunk to house the lower furnace insulating plug. The testpiece rested on a pedestal with three posts that were bolted to the stainless steel plate.

On the back plate of the translation platform were mounted three ball bushing pillow blocks. To eliminate the possibility of binding during transit, two bushings were placed on one side of the platform and one on the other. A stainless steel cable connected to the back of the platform facilitated manual translation of the testpiece aided by a counterweight.

After proper heating, the testpiece was lowered into the spray chamber where it was quenched. The spray chamber frame was constructed of carbon steel and coated with epoxy paint. One aluminum plate was mounted on each side of the chamber, allowing for flexibility in the mounting of spray nozzles and the connection of water hoses leading to the nozzles. Optical grade Lexan sheets covered the remainder of the spray chamber. These not only contained the sprayed water, but they also provided visual access to the quench.

Steam produced by the quench was removed by an exhaust system placed on top of the spray chamber. The steam was confined in a Lexan hood placed above the spray chamber. Attached to one side of the hood was a galvanized steel duct, inside which a small fan helped reject the steam to a nearby window.

Water used in the test bed was stored in a large tank at the bottom of the test bed frame. This tank was fabricated from aluminum sheet and painted with epoxy paint. From the tank, the

water was circulated by a totally enclosed, fan-cooled centrifugal pump. The large capacity of the pump required bypassing most of the flow to maintain flow stability. The main flow then passed through a 5- μ m filter followed by a heat exchanger before entering steel-reinforced rubber hoses ending each with a spray nozzle. Flow into each nozzle was regulated with a bronze globe valve, and nozzle pressure was read from a pressure gage. After impinging on the testpiece inside the spray chamber, the water was collected in the tank for recirculation.

2.2 Testpiece

The L-shape testpiece (Fig. 5) was constructed of Al 1100-O. It allowed investigation of the effects of part shape and varying section thickness on a quenched part. Other effects were definitely present, such as water run-off and spray interference, but these were not the central issues for this study.

Section thickness in the L-shape testpiece was approximately two-to-one. Eleven type K thermocouples were embedded in the testpiece at locations that were chosen to minimize disturbance to isotherms and to accurately track the temperature response at crucial points. The thermocouples were placed in a plane 6.03 cm (2 $\frac{3}{8}$ in.) above the lower surface of the L-shape testpiece, as shown in Fig. 5, to measure the temperatures near the midplane of the lower spray. Uniform surface roughness was achieved by blasting the surfaces to be quenched with fine silica particles.

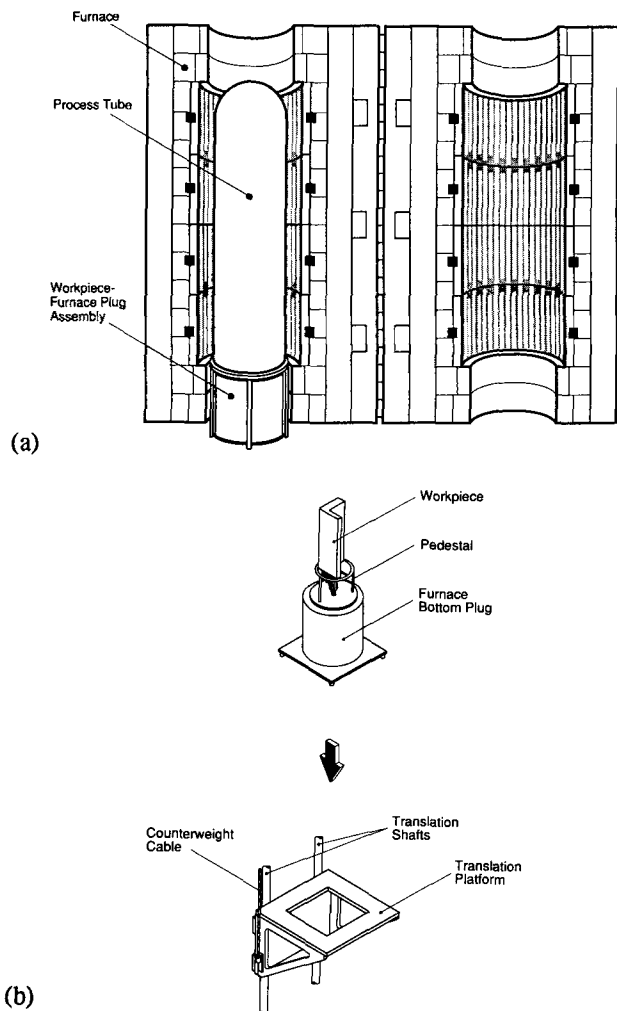


Fig. 4 Schematic of (a) process tube placement inside the furnace and (b) testpiece support assembly.

2.3 Experimental Procedure

Testing commenced with the raising of the testpiece into the furnace using the translation platform. The testpiece went through a controlled heat-up to a uniform temperature. Once the testpiece reached the desired initial temperature, approximately 550 °C, the sprays were initiated and allowed to reach hydrodynamic equilibrium. The testpiece was then lowered into the spray chamber, and temperatures were recorded using a Keithley 500 data acquisition system interfaced to a Compaq Deskpro 386 microcomputer. Recording of the temperatures was optimized to allow the maximum amount of data to be collected. Temperatures were recorded every 1 sec in the film boiling and single-phase regimes and every 200 msec in the transition and nucleate boiling regimes.

3 Experimental Results

The sprays were arranged and the testpiece was designed in such a way as to ensure the geometrical placement of the test-

piece within the spray chamber. This was done to ensure complete coverage of each of the quenched surfaces by the water sprays, while minimizing spray interference. Two different spray configurations were considered. In the first configuration, Case A quench, the two outer vertical surfaces of the L-shape testpiece were each quenched with two flat sprays. The second configuration, Case B quench, consisted of quenching the two outer surfaces as with Case A, as well as the inner vertical surface of the thick section. Because the spray field of a flat spray takes the form of an oval with a large major-to-minor axis ratio, the two sprays on each sprayed surface were placed one above the other such that their major axes coincided with the vertical centerline of the corresponding quenched surface. Temperature measurements were obtained in a plane perpendicular to the quenched surface, but passing through the minor axis of the lower spray field. The spray nozzles were located a distance of 30.48 cm (12.0 in.) from the respective sprayed surfaces, the test pressure was 551 kPa (80 psi), and the water temperature was 23 °C.

Figure 6(a) shows temperature-time quench curves for various points in the L-shape corresponding to the Case A quench. Several observations can be made concerning these curves. Most evident is the fact that thermocouple TC5, located within the thin section, quenched much more quickly than thermocouple TC3, located at the center of the thick section. This result is to be expected because of the decreased thermal mass in the thin section. Because of the low volumetric flux, Q'' , near the edges of the spray, thermocouple TC1 quenched more slowly than TC2. This phenomenon indicates that spatial variations in the spray flux distribution can cause large temperature gradients near the surface, resulting in uneven cooling and contributing to the occurrence of points of low hardness and poor strength.

Perhaps a more subtle observation is the width of the quench band in time. At its widest, the quench band was approximately 180 °C wide. This points to the existence of substantial thermal gradients within the material, possibly causing poor mechanical properties and warpage.

Results for Case B, shown in Fig. 6(b), reveal that points corresponding to thermocouples TC5 and TC3 quench in a very similar manner, indicating a uniformity of temperature response between the thick and thin sections of the testpiece. Also, the quench band was much thinner than for Case A.

The temperature-time envelopes of Case A and Case B are compared in Fig. 7. Not only was the quench band much thinner in Case B, but the entire quench proceeded much faster. This is extremely desirable, because a rapid, uniform quench will result in enhanced and more uniform mechanical properties than a slower, uneven quench.

Figure 7 indicates that the placement of the spray nozzles has a large effect on the resulting temperature-time response of the quenched part. Proper configuration of the nozzles can result in a quench that proceeds in a uniform and rapid manner, providing increased final hardness and reduced residual stresses.

4 Numerical Results

Because the actual experiments involved three-dimensional effects and a spatially varying boundary condition, the following two-dimensional numerical model is not presented for exact

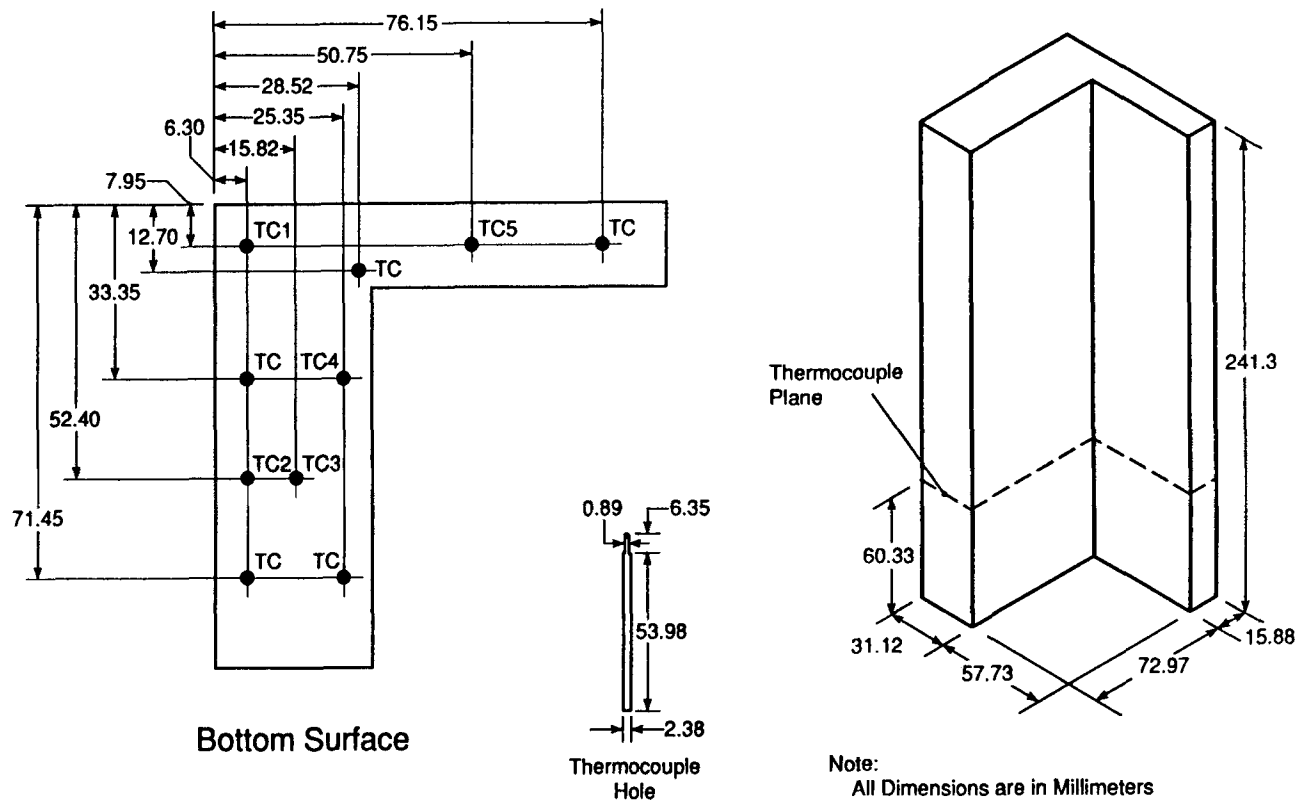


Fig. 5 L-shape testpiece dimensions and thermocouple placement.

simulation of the quench. Rather, the ANSYS numerical results are presented as a medium to allow for the assessment of trends concerning the optimization of spray configuration in a simulated quench of an aluminum part made of Al 1100-O and an initial attempt to calculate hardness in a simulated quench of an aluminum part made of alloy 2024-T6. To investigate the influence of spray configuration on temperature-time results and hardness, the L-shape was chosen because of its sections of differing thickness, which enables general findings from the present work to apply to testpieces having irregular geometries. The numerical domain for the simulated quenching of the L-shape part corresponding to Case A and Case B are shown in Fig. 8(a) and (b), respectively.

The most difficult task in the development of the computational model was the characterization of the boundary conditions. The spray heat transfer coefficient varied in both space and time, so special care had to be taken when deciding how to correctly apply this type of boundary condition to the model.

The boundary condition was applied to the model through the use of a macro, a subroutine feature of the ANSYS computer code, via the following steps. First, the temperatures of the sprayed surface were obtained from a previous solution step. Second, two surface nodes were selected, and their temperatures and spatial locations were sent to the macro. Third, the macro took the average of both the nodal temperatures and locations to obtain the average temperature for the exposed boundary of a given surface element and to assign this temperature to the middle of the surface element boundary. The average locations were

then used to calculate the spray hydrodynamic parameters (*i.e.*, Q'' , U_m , and d_{32}) using the curve fits of Deiters and Mudawar^[10] to the spatial distributions measured for each of the parameters for a spray nozzle of the same part number as that used in the present study and for similar spray pressure and nozzle-to-surface distance. Note that for the numerical domain of interest, the volumetric flux distribution determined by Deiters and Mudawar is skewed slightly. This skewed distribution was obtained for a particular placement of the nozzle relative to the sprayed surface. Both in the quenching test bed and the numerical modeling care was taken to place the nozzles relative to the testpiece in a consistent manner. This procedure assumes, of course, that the spray hydrodynamic parameters measured and curve fitted by Deiters and Mudawar were identical to those of the present study. Due to tolerances in the fabrication of the spray nozzles this was, most likely, not the case. However, this approximation was sufficient for the purposes of the present numerical model. These spray hydrodynamic parameters and the average element temperatures were then used to calculate a heat transfer coefficient using the correlations developed by Mudawar and Valentine,^[7] Klinzing,^[8] and Rozzi,^[9] which are summarized in Table 1. Finally, this heat transfer coefficient was applied to the entire exposed boundary of the surface element, as specified by the aforementioned nodes. For the unsprayed surfaces, both free convection with air and radiation losses were taken into account. Then, an equivalent heat transfer coefficient was calculated, which was found to be insignificant compared to the heat transfer coefficients experienced on the quenched surfaces. A new

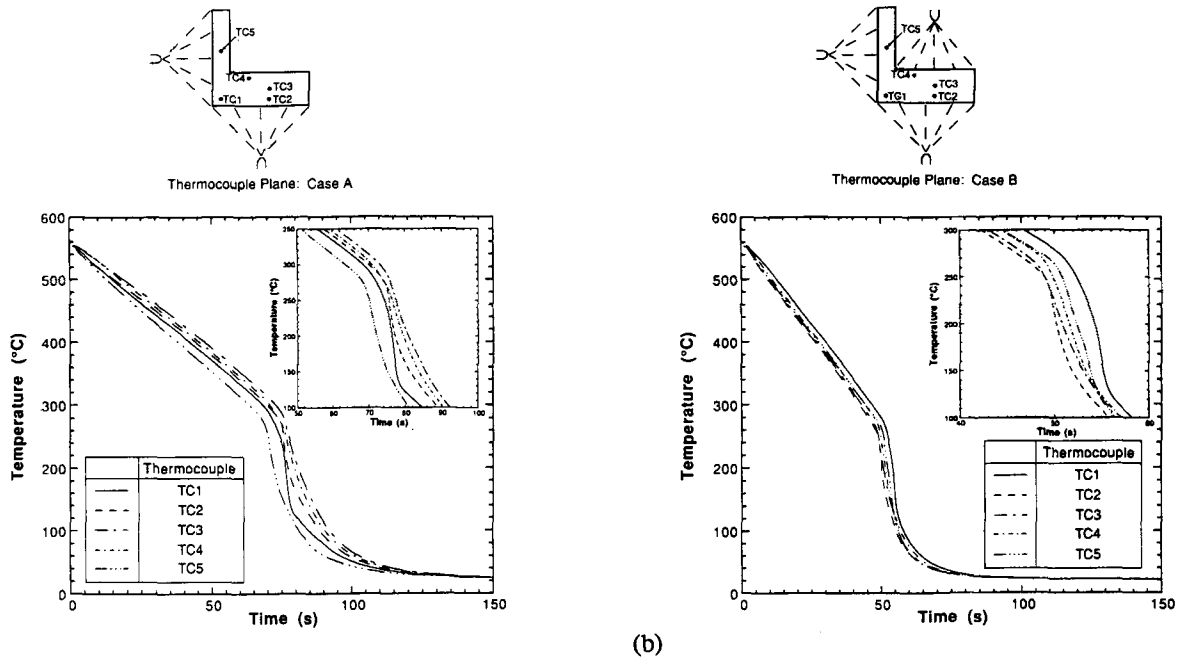


Fig. 6 Measured temperature-time curves for (a) Case A and (b) Case B quench of aluminum 1100-O testpiece.

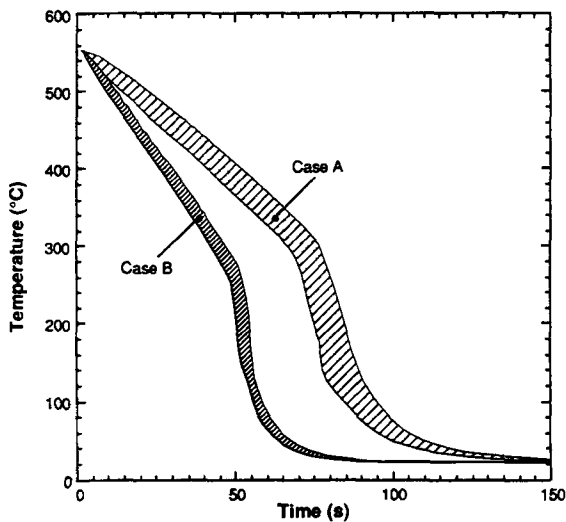


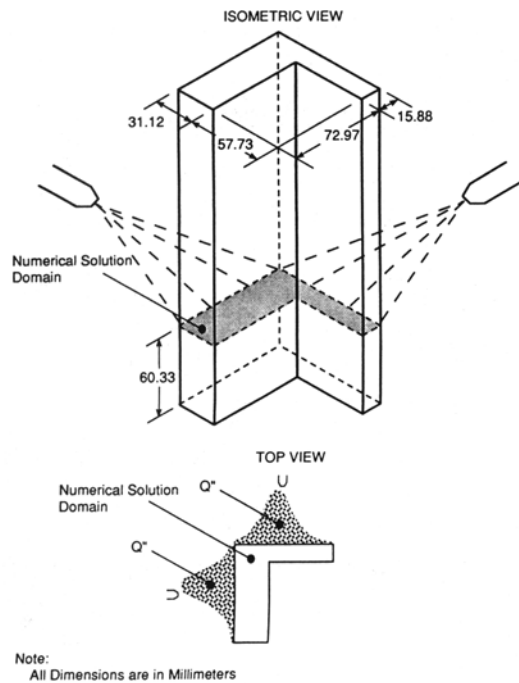
Fig. 7 Comparison of the measure temperature envelopes for Case A and Case B quench of aluminum 1100-O testpiece.

heat transfer coefficient was then calculated for the exposed surface of each surface element at the beginning of each new increment of time.

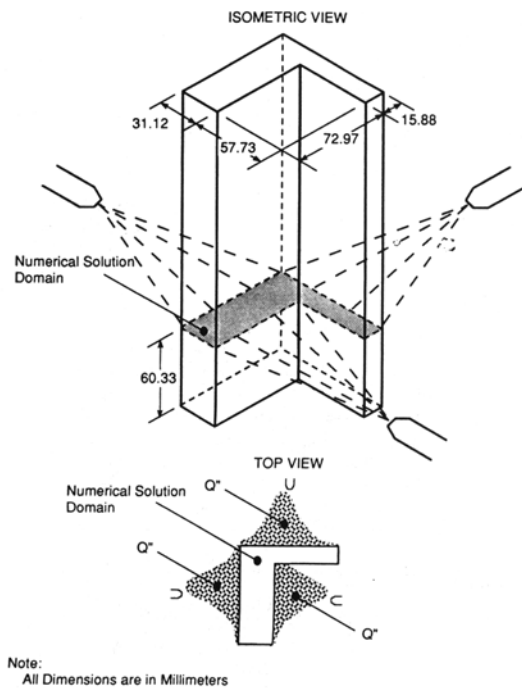
4.1 Temperature Predictions

The two-dimensional model was used only for the purpose of assessing general trends concerning the quenching of the aluminum 1100-O L-shape testpiece for a Case A and Case B quench.

Figures 9(a) through (d) show isotherm plots for Case A. For the first plot (Fig. 9a), the sprayed surface of the thin section was in film boiling. One can note that there were large temperature differences between the thick and thin sections. Although the thin section approached temperature uniformity, temperature differences as large as 85 °C existed in the thick section. Also, the skewed distribution of volumetric spray flux for each spray manifested itself in the off-center location of the point of minimum temperature on each sprayed surface. This had its greatest effect on the thick section, causing more heat to be drawn toward the thin section. These trends continued as the sprayed surface of the thin section reached transition boiling, as shown in Fig. 9(b). Because of the low temperature within the thin section and the lagging of the thick section in departure from film boiling, heat was drawn almost directly to the thin section, decreasing the effectiveness of the spray on the thick section and increasing the temperature difference in the thick section to as much as 240 °C. When single-phase cooling was finally established on the sprayed surface of the thin section (Fig. 9c), nucleate boiling was beginning to develop on the sprayed surface of the thick section closest to the thin section, whereas the remaining part of the sprayed surface was still lagging behind undergoing transition boiling. Because of the massive heat transfer associated with nucleate boiling, the sprayed surface of the thick section became a more favorable path for heat flow. This reduced the temperature gradients in the thick section considerably. Figure 9(d) shows a temperature distribution well into the quench as both sprayed surfaces had entered the single-phase cooling regime. Note that, in all cases, there was minimal heat flow into the unsprayed surfaces as evidenced by the isotherms perpendicular to the surface, proving that the unsprayed surfaces behave as virtually insulated boundaries.



(a)



(b)

Fig. 8 Numerical domain for (a) Case A and (b) Case B quench of aluminum 1100-O testpiece.

The isotherm plots for a Case B quench posed a much more desirable cooling situation, as indicated in Fig. 10(a) through 10(d). In general, the quench proceeded with small temperature gradients in the testpiece. Like Case A, there was virtually no heat flow from the unsprayed surfaces in either the thick or thin sections. Additionally, the skewed volumetric flux distribution caused departure of the minimum temperature locations from the geometrical center of each spray. This is most evident in Fig. 10(a), in which the sprayed surface of the thin section was in film boiling. Aided by the large surface area-to-volume ratio, the skewed volumetric flux distribution of the spray caused premature cooling at the lower left corner and increased the heat flow across each section toward the minimum temperature points for each surface. Nevertheless, temperature approached uniformity throughout the testpiece, and the large temperature gradients found in Case A were virtually eliminated. These trends continued in Fig. 10(b), in which the sprayed surface of the thin section has entered transition boiling. Temperature differences between the corner region of the testpiece and the outer edges of both the thick and thin sections increased, causing significant heat flow toward the corner. These trends also prevailed as the sprayed surface of the thin section entered nucleate boiling, as shown in Fig. 10(c). However, temperature was again fairly uniform throughout the testpiece. Figure 10(d) shows the temperature distribution as all the sprayed surfaces entered the single-phase cooling regime. As shown by the temperature predictions, particularly for testpieces having sections of differing thicknesses, the spray configuration has a pronounced effect on the subsequent uniformity of the quench.

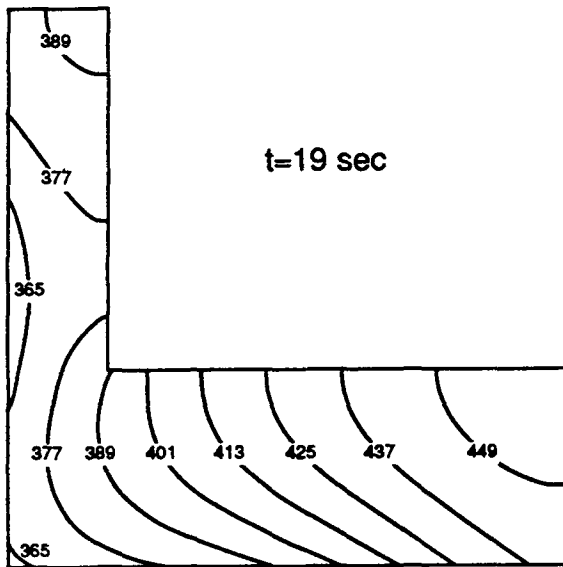
The aforementioned discussion raises an important issue concerning the accurate representation of spray properties, par-

ticularly volumetric flux. For a quenching process to be predictable and repeatable, tolerances will have to be tightly controlled in the fabrication of spray nozzles. Alternatively, before using a particular nozzle, its performance must be carefully examined and its spray parameters fully characterized. One of these two methods must be used if accurate modeling is to be realized in any quenching process.

4.2 Hardness Predictions

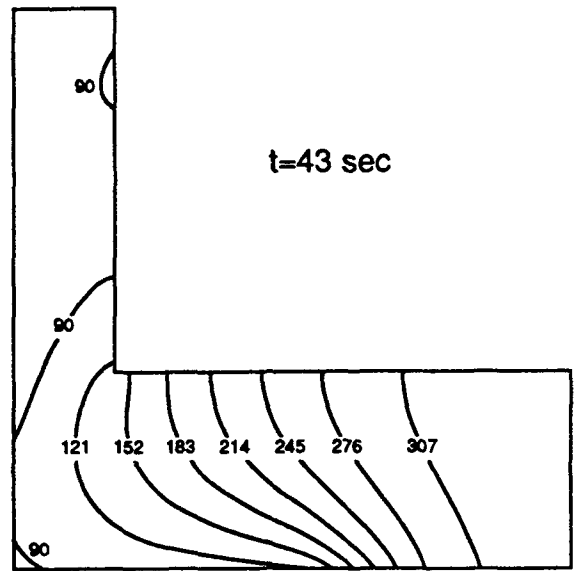
Quenching of the L-shape testpiece was also simulated numerically for the case of aluminum alloy 2024-T6 to compare the effects of a Case A and Case B quench on the testpiece hardness. ANSYS was first used to obtain temperature-time curves for the simulated quench. Then, by using the C-curve for Al 2024-T6,^[5] the final hardness was calculated using the quench factor technique discussed earlier. The physical dimensions and spray boundary conditions for this model were exactly the same as those of the commercially pure aluminum 1100-O L-shape testpiece.

Hardness results for a Case A quench of the 2024-T6 testpiece are shown in Fig. 11(a). Many interesting observations can be made concerning these results. The upper part of the thin section seems to acquire a relatively uniform hardness. This makes intuitive sense, because this section should quench more rapidly and uniformly because of its small thermal mass. Because of its larger thermal mass and the imposed spray configuration, the thick section quenched more slowly, resulting in a lower hardness compared to the thin section. However, what was not expected was the relatively large hardness on the unsprayed



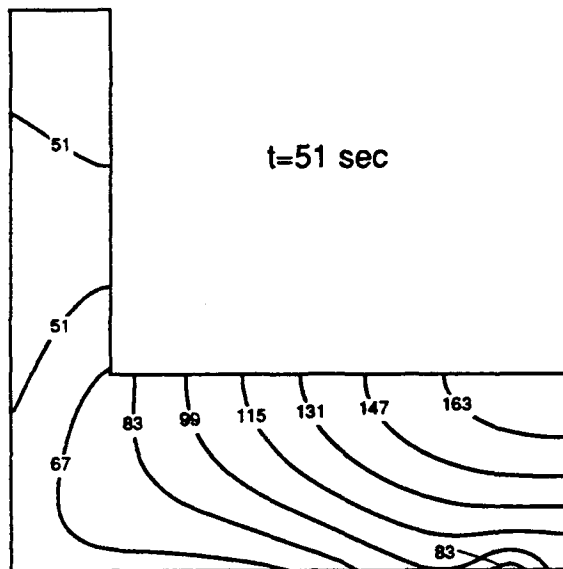
Sprayed Surface of Thin Section Undergoing Film Boiling

(a)



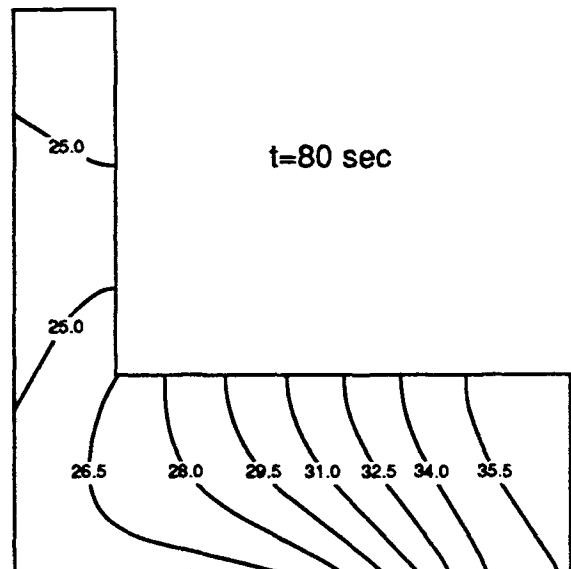
Sprayed Surface of Thin Section Undergoing Transitional Boiling

(b)



Sprayed Surface of Thin Section Undergoing Nucleate Boiling

(c)



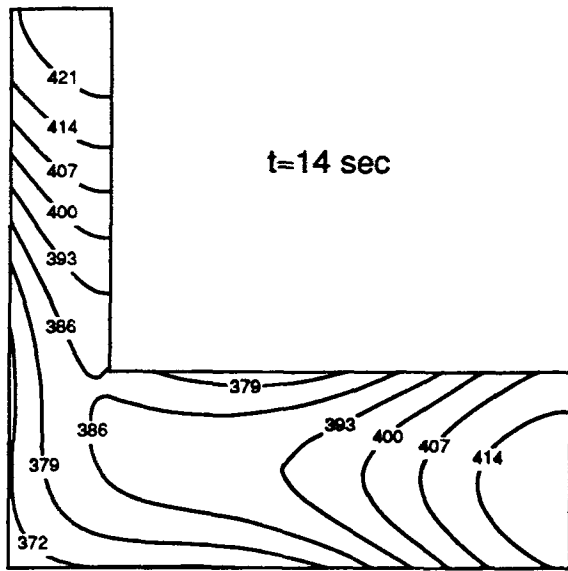
Sprayed Surface of Thin Section Undergoing Single-Phase Cooling

(d)

Fig. 9 Numerically predicted temperature distribution for selected times during a Case A quench of aluminum 1100-O testpiece.

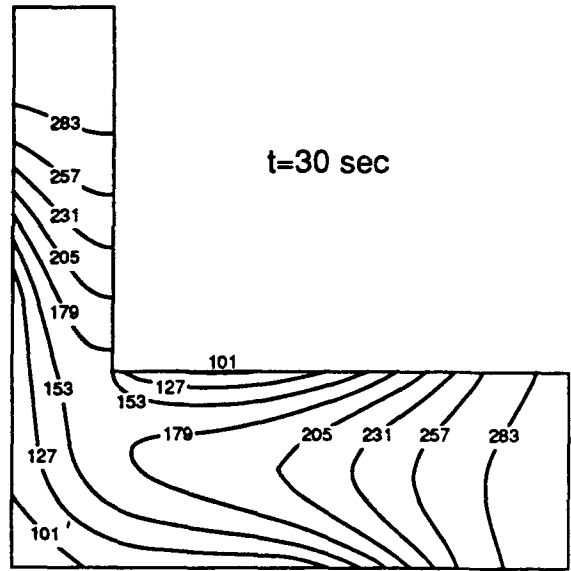
boundary of the thick section compared to the sprayed boundary of the same section. This phenomenon is explained in Fig. 12, which shows a portion of the quench curve for both a sprayed and an unsprayed surface node on the thick section of the test-

piece. Although the sprayed node proceeded through the *C*-curve first, the unsprayed node traversed it much faster. Because the quench factor is directly proportional to the time it takes for the quench curve to proceed through the *C*-curve, *i.e.*:



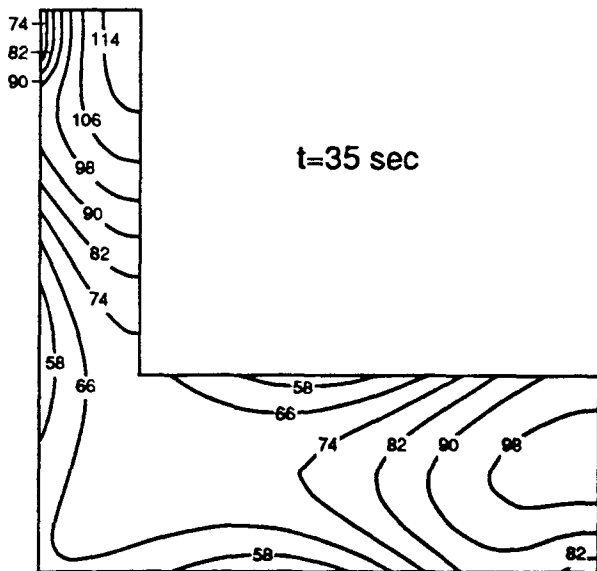
Sprayed Surface of Thin Section Undergoing Film Boiling

(a)



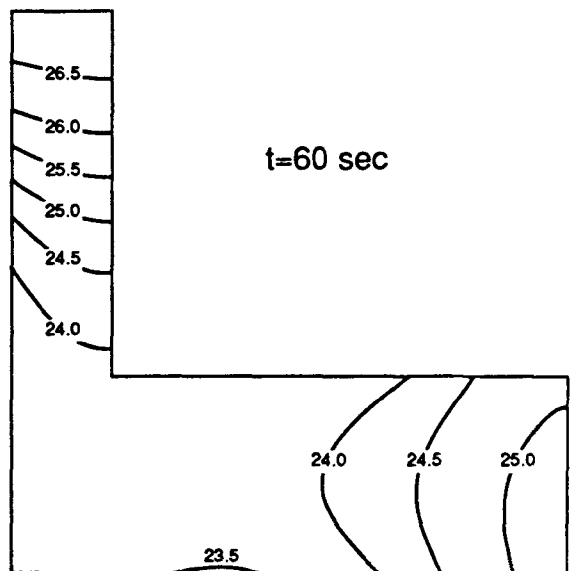
Sprayed Surface of Thin Section Undergoing Transitional Boiling

(b)



Sprayed Surface of Thin Section Undergoing Nucleate Boiling

(c)



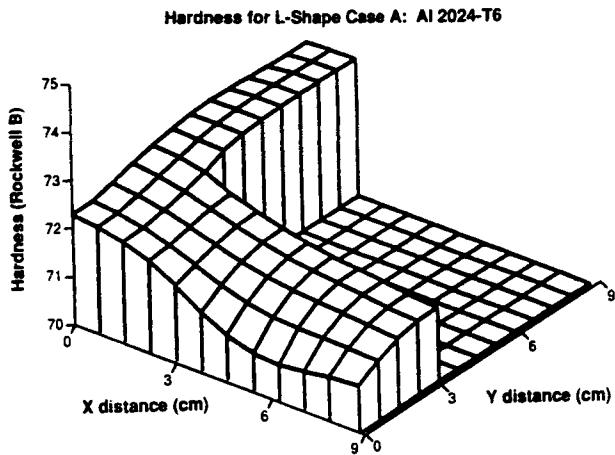
Sprayed Surface of Thin Section Undergoing Single-Phase Cooling

(d)

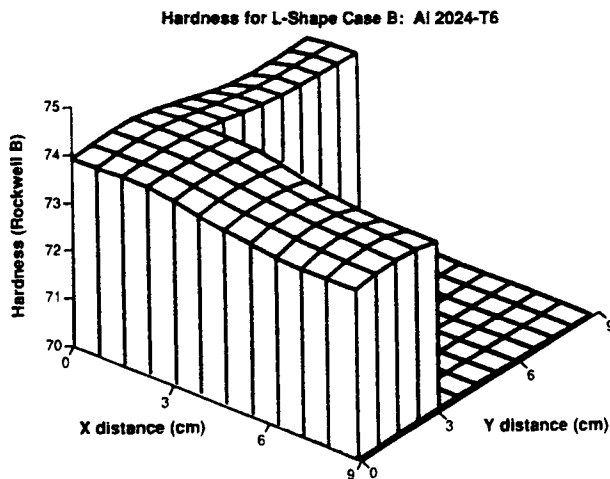
Fig. 10 Numerically predicted temperature distribution for selected times during a Case B quench of aluminum 1100-O testpiece.

$$\tau = \frac{\Delta t_1}{C_1} + \frac{\Delta t_2}{C_2} + \dots + \sum_1^{N-1} \frac{\Delta t_N}{C_N} \quad [7]$$

the quench factor is higher and the hardness lower for the sprayed surface.



(a)



(b)

Fig. 11 Hardness for a (a) Case A and (b) Case B numerically simulated quench of aluminum alloy 2024-T6 testpiece.

Figure 11(b) shows the hardness results for a Case B quench of the aluminum Al 2024-T6 testpiece. Because the quench was more rapid than in Case A, the final hardness was increased compared to Case A. Because of the uniformity of the quench, the hardness was also more uniform throughout the testpiece because of the spatial uniformity in temperature during the quench. This same uniformity is proof that a Case B quench would aid in the reduction of residual stresses of the part produced.

In developing the means to optimize the quenching process, accurate simulation of the quench and its consequences is a vital step. The present results indicate that the material properties of

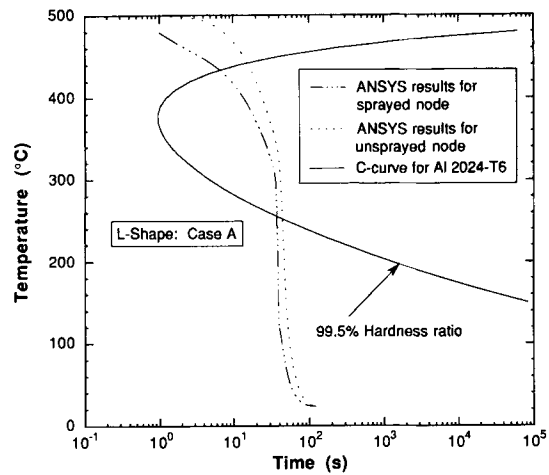


Fig. 12 Comparison of selected quench curves predicted from the numerical model and the C-curve for aluminum alloy 2024-T6.

parts with irregular shapes and differing section thicknesses can be assessed prior to the quench itself, providing the means to find the ideal nozzle configuration.

Acknowledgments

Financial support for this work by the Purdue University Engineering Research Center for Intelligent Manufacturing Systems is gratefully appreciated. The authors thank Jerry Hagers and Rudolf Schick of Spraying Systems Co. and Gerry Dail of ALCOA for their valuable technical assistance.

References

1. J.F. Shackelford, *Introduction to Materials Science for Engineers*, Macmillan Publishing, New York (1985).
2. S.J. Chevrier, A. Simon, and G. Beck, Optimal Cooling Rate and Process Control in Metallic Parts Heat Treatment, in *Heat and Mass Transfer in Metallurgical Systems*, vol 9, 535-544 (1981).
3. J.W. Evancho and J.T. Staley, Kinetics of Precipitation in Aluminum Alloys during Continuous Cooling, *Met. Trans.*, 5, 43-47 (1974).
4. J.W. Cahn, Transformation Kinetics during Continuous Cooling, *Acta Metall.*, 4, 572-575 (1956).
5. J.S. Kim, "Prediction of the Influence of Water Spray Quenching on the Age-Hardenability of Aluminum Alloy 2024," M.S. thesis, Purdue University, West Lafayette, IN (1989).
6. C.E. Bates, Predicting Properties and Minimizing Residual Stress in Quenched Steel Parts, *J. Heat Treat.*, 6, 27-45 (1988).
7. I. Mudawar and W.S. Valentine, Determination of the Local Quench Curve for Spray-Cooled Metallic Surfaces, *J. Heat Treat.*, 7, 107-121 (1989).
8. W.P. Klinzing, "Development of the Spray Quenching Test Bed and Correlations for the Film Boiling Regime," M.S. thesis, Purdue University, West Lafayette, IN (1991).
9. J.C. Rozzi, "Quenching of Aluminum Parts Having Irregular Geometries Using Multiple Water Sprays," M.S. thesis, Purdue University, West Lafayette, IN (1991).
10. T.A. Deiters and I. Mudawar, Prediction of the Temperature-Time Cooling Curves for Three-Dimensional Aluminum Products during Spray Quenching, *J. Heat Treat.*, 8, 81-91 (1990).